Eidgenössische Technische Hochschule Zürich

Ecole polytechnique fédérale de Zurich
Politecnico federale di Zurigo
Swiss Federal Institute of Technology Zurich

Multilevel Monte Carlo for two phase flow and transport in random heterogeneous porous media

F. Müller, P. Jenny and D.W. Meyer

Research Report No. 2012-12
May 2012

Seminar für Angewandte Mathematik
Eidgenössische Technische Hochschule
CH-8092 Zürich
Switzerland

Multilevel Monte Carlo for Two Phase Flow and Transport in Random Heterogeneous Porous Media

Florian Müller[1,*], Patrick Jenny[1], Daniel W. Meyer[1]

Abstract

Monte Carlo (MC) is a well known method for quantifying uncertainty arising for example in subsurface flow problems. Although robust and easy to implement, MC suffers from slow convergence. Extending MC by means of multigrid techniques yields the multilevel Monte Carlo (MLMC) method. MLMC has proven to greatly accelerate MC for several applications including stochastic ordinary equations in finance, elliptic stochastic partial differential equations and also hyperbolic problems. In this study, MLMC is combined with a streamline-based solver to assess uncertain two phase flow and transport in random heterogeneous porous media. The performance of MLMC is compared to MC for a two dimensional reservoir with multi-point Gaussian logarithmic permeability fields. The influence of the variance and the correlation length of the logarithmic permeability on the MLMC performance is studied.

Keywords: Multilevel Monte Carlo, Random heterogeneous porous media, Two phase flow, Two phase transport, Streamline solver

1. Introduction

The simulation of subsurface two phase transport, or more precisely of oil water flow and transport in heterogeneous porous media, is plagued by a lack of information concerning the permeability field. Usually, permeability measurements are only available at few locations in the reservoir and as a consequence, stochastic permeability models are introduced [1]. To determine the uncertainty in the transport resulting from the uncertainty of the permeability, probabilistic methods are deployed.

In single phase subsurface flow problems arising in hydrology, probabilistic collocation and probabilistic Galerkin methods have been successfully applied to quantify the resulting pressure uncertainty [2]. Application of the same methods

*Tel.: +41 44 633 9249; fax: +41 44 632 1104.
Email addresses: florian.mueller@sam.math.ethz.ch (Florian Müller), jenny@ifd.mavt.ethz.ch (Patrick Jenny), meyerda@ethz.ch (Daniel W. Meyer)
[1]Institute of Fluid Dynamics, Sonneggstrasse 3, ETH Zurich, Zurich CH-8092, Switzerland

for flow and transport is more challenging as was demonstrated in [3]. Alternatively, in [4] probabilistic collocation for flow was combined with a streamline-based Monte Carlo (MC) method for transport to obtain accurate predictions for the transport uncertainty. In order to obtain predictions at acceptable computational costs, probabilistic collocation/Galerkin rely on a parametric representation of the random permeability in terms of a few scalar random variables. The Karhunen-Loeve (KL) expansion used for example in [2, 3, 4] can provide such a low dimensional representation for permeability fields with long correlation lengths with respect to the size of the reservoir domain. Unfortunately, realistic permeability fields for oil reservoirs have rather short correlation lengths and therefore, KL-based probabilistic collocation/Galerkin methods are of limited applicability.

Zhang and coworkers [5, 6] have derived saturation mean and variance equations based on Lagrangian streamline techniques. Their equations are based on moments of the travel time and transverse displacement which are determined by means of a presumed joint PDF. Their approach was first formulated for one dimensional and two dimensional flows with space-stationary flow statistics [5]. In the one dimensional case, the porosity was a random field whereas in the two dimensional case permeability was uncertain. In a subsequent work [6], an extension for more complex flow scenarios was provided where the Lagrangian travel time and displacement statistics are calculated numerically. The two dimensional derivations of Zhang and coworkers are based on the assumption that the logarithmic permeability standard deviation is moderately high. Moreover, they assume that the flow field that determines the streamlines is time-independent or more specifically not influenced by saturation changes. Similarly, one can assume that the streamline pattern or geometry is time-independent. In this work, we refer to this less restrictive assumption as the fixed streamline assumption.

The MC method is general and straight forward to apply for oil reservoir problems with uncertain heterogeneous permeability. However, MC suffers from slow statistical convergence which necessitates a large number of sample solutions. Each sample is comprised of a flow and a transport solution for one random permeability field realization. Since the partial differential equations (PDEs) that determine the flow and transport problem are rather involved, MC is computationally expensive.

To reduce the computation cost of MC, the multilevel Monte Carlo (MLMC) method was introduced. In MLMC, multigrid techniques are applied. More precisely, the stochastic quantity of interest, in our case the solution of a stochastic PDE system, is represented on grids of varying resolutions. When estimating statistical moments of the solution, samples on all grid levels are taken into account. In this process, the samples on coarser grids, which capture coarse-scale solution features, are calculable at greatly reduced computational expenses compared to samples on the finest grid. In conventional MC all samples are generated on the finest grid.

The MLMC method was introduced by Heinrich in the context of parametric integration [7]. Among other contributions, Giles has used MLMC for path simulations of stochastic ordinary differential equations [8]. Recently, MLMC

was applied for the solution of the elliptic pressure problem in the context of subsurface flow [9]. Schwab et al. have performed a theoretical analysis of MLMC and have provided numerical examples involving elliptic PDEs [10] and hyperbolic conservation laws [11, 12].

In the present work, we apply MLMC for two phase transport simulations of an oil reservoir with uncertain heterogeneous permeability. For phase transport, a streamline technique is used with and without the fixed streamline assumption. Streamline-based transport solvers are well established in the petroleum engineering community [13]. The performance of MLMC is compared to conventional MC for different permeability variances or heterogeneity levels and correlation lengths. Moreover, the validity of the fixed streamline assumption is assessed.

The remainder of the paper is organized as follows. First, Sections 2 and 3 present the PDE model for oil water transport in heterogeneous porous media and the streamline solver. A discussion on the characterization of the uncertain permeability field is provided in Section 4. Section 5 introduces the MLMC technique. Test cases for numerical experiments are specified in Section 6 and details on the numerical solution method are provided in Section 7. Finally, Section 8 contains a discussion of the numerical results and conclusions are drawn in Section 9.

2. Problem Formulation

Incompressible immiscible displacement of oil by water in a heterogeneous reservoir is considered. The problem formulation outlined in this section is based on Section 'General Mathematical Statement' of [5]. Water is assumed to be the wetting phase whereas oil is non wetting. In the absence of source terms, the mass conservation of water reads

$$\phi \frac{\partial S_w}{\partial t} + \nabla \cdot \boldsymbol{q}_w = 0. \tag{1}$$

Here, ϕ denotes the porosity, S_w the water saturation and $S_o = 1 - S_w$ is the saturation of the oil phase. If capillary pressure and gravity are neglected, the water flux $\boldsymbol{q}_w$ is given by

$$\boldsymbol{q}_w = -\lambda_w \nabla p,$$

with p being the pressure. The water mobility λ_w is modeled as

$$\lambda_w = k \frac{k_{r,w}}{\mu_w}.$$

λ_w depends on the spatially varying absolute permeability k and the water relative permeability $k_{r,w}$ which is a function of water saturation S_w only. μ_w is the viscosity of water.

Continuity is ensured by

$$\nabla \cdot \boldsymbol{q}_{tot} = 0, \tag{2}$$

where the total flux $\boldsymbol{q}_{tot}$ is defined as

$$\boldsymbol{q}_{tot} = \boldsymbol{q}_w + \boldsymbol{q}_o.$$

Introducing the total mobility λ_{tot},

$$\lambda_{tot} = \lambda_w + \lambda_o,$$

the total flux becomes

$$\boldsymbol{q}_{tot} = -\lambda_{tot} \nabla p, \tag{3}$$

and the continuity equation (2) can be written as

$$-\nabla \cdot (\lambda_{tot} \nabla p) = 0. \tag{4}$$

Introducing the fractional flow function for water,

$$f_w = \frac{\lambda_w}{\lambda_{tot}} = \frac{k_{r,w}/\mu_w}{k_{r,w}/\mu_w + k_{r,o}/\mu_o},$$

equation (1) changes to

$$\phi \frac{\partial S_w}{\partial t} + \boldsymbol{q}_{tot} \cdot \nabla f_w = 0. \tag{5}$$

In summary, the propagation of S_w is governed by pressure equation (4) and transport equation (5). Since λ_{tot} depends on S_w, the two equations are coupled.

3. Streamline Solver

In this work, a Lagrangian streamline solution method is applied to solve the saturation transport equation (5). The streamline solver presented in this section is based on [14, 15].

Under the fixed streamline assumption, which implies that the total flux $\boldsymbol{q}_{tot}$ direction does not change over time, a streamline $\boldsymbol{x}_{sl}(\tau)$ originating from point $\boldsymbol{x}_{0,sl}$ is defined as

$$\boldsymbol{x}_{sl}(\tau) = \boldsymbol{x}_{0,sl} + \int_0^\tau \boldsymbol{q}_{tot}(\boldsymbol{x}_{sl}(\tau'))d\tau', \tag{6}$$

where τ is the so-called time of flight. Based on streamlines that are surrounding streamline $\boldsymbol{x}_{sl}(\tau)$, a streamtube with cross-sectional area $A(\tau)$ can be defined. With the streamline travel distance defined as $dr = |\boldsymbol{q}_{tot}|d\tau = q_{sl,tot}/A\, d\tau$, equation (5) can be rewritten along a streamline as

$$\phi A \frac{\partial S_w}{\partial t} + q_{sl,tot} \frac{\partial f_w}{\partial r} = 0. \tag{7}$$

Moreover, with the total volumetric flux $q_{sl,tot}$, the continuity equation along a streamline can be written as

$$\frac{\partial q_{sl,tot}}{\partial r} = 0. \tag{8}$$

Similar to equation (3), $q_{sl,tot}$ can be expressed as

$$q_{sl,tot} = -A\lambda_{tot}\frac{\partial p}{\partial r}, \tag{9}$$

based on the pressure gradient along a streamline.

By introducing the cumulative injection volume Q and the cumulative pore volume V, i.e.,

$$\begin{aligned} Q(t) &= \int_0^t q_{sl,tot}(t')dt' \quad \text{and} \quad dQ = q_{sl,tot}dt, \text{ and} \\ V(r) &= \int_0^r \phi(r')A(r')dr' \quad \text{and} \quad dV = \phi A dr, \end{aligned} \tag{10}$$

equation (7) can be written as a simple Buckley-Leverett equation,

$$\frac{\partial S_w}{\partial Q} + \frac{\partial f_w}{\partial V} = 0. \tag{11}$$

For more details on this step we refer to [15]. Since $q_{sl,tot}$ is independent of r along a streamline (see equation (8)), equation (9) can be rearranged and integrated from streamline location $r = 0$ to L with pressures $p(t, r = 0) = p_0$ and p_L, respectively, which leads to

$$\begin{aligned} \int_{p_0}^{p_L} dp &= q_{sl,tot}\int_0^L \frac{1}{-A\lambda_{tot}}dr \\ \Rightarrow q_{sl,tot} &= \frac{\Delta p}{R} \text{ with } R = \int_0^L \frac{1}{A\lambda_{tot}}dr. \end{aligned} \tag{12}$$

R is a saturation-dependent resistance and $\Delta p = p_L - p_0$.

To relax the fixed streamline assumption invoked at the beginning of this section, an iterative method is commonly applied [13]. Here, the pressure and saturation are updated in subsequent steps according to equations (4) and (7), respectively. After having updated the pressure field, the streamline pattern changes based on equations (3) and (6). More details on the streamline solution algorithm are provided next.

3.1. Streamline Solution Algorithm

In this work, we focus on a scenario where pressure boundary conditions are specified at in- and outflow with Δp being provided.

The total simulation time is divided into time steps of two different categories. The global time step size Δt_g is used for updating the global pressure

field within the reservoir. A change in global pressure is coupled with an update of the streamline pattern. Each time step Δt_g is subdivided into smaller intermediate time steps of size Δt_i. The total mobility λ_{tot} or rather the resistance R along a streamline is updated in steps of Δt_i.

For a given initial water saturation S_w and time steps Δt_g and Δt_i, the flow and transport problems are solved according to the following algorithm.

1. Based on S_w, the global pressure problem is solved (equation (4)) and $\boldsymbol{q}_{tot}$ is determined. For this purpose, a finite volume (FV) method in connection with an algebraic multigrid solver is used [16].
2. According to $\boldsymbol{q}_{tot}$, a streamline family is generated according to Pollock's algorithm [17]. The streamline grid cells Δr are not equally spaced and are determined by the intersections of the streamline with the FV grid.
3. The properties ϕ, k and S_w are assigned to every streamline cell and $|\boldsymbol{q}_{tot}|$ to every streamline cell interface.
4. The initial flux $q_{sl,tot}$ is set to the arbitrary value 1. Based on $A(r) = q_{sl,tot}/|\boldsymbol{q}_{tot}(r)|$, $A(r)$ along each streamline is determined correctly up to a constant factor.
5. For every streamline cell, $\Delta V = \int_{\Delta r} \phi A dr'$ is numerically calculated and Q is initialized to 0.
6. The resistance R and the volume injected during the time step Δt_i are numerically calculated based on equation (12) and $\Delta Q = \int_{\Delta t_i} q_{sl,tot} dt' \approx \Delta t_i \, \Delta p/R$, respectively.
7. The water saturation S_w is updated along streamlines based on the solution of the Buckley-Leverett equation (11) and the cumulative volume injected $Q = Q + \Delta Q$. Note that the Buckley-Leverett solution is independent of the choice of the initial $q_{sl,tot}$ from step 4 since both Q and V are proportional to A.
8. Steps 6 and 7 are repeated until the intermediate time steps Δt_i add up to the global time step Δt_g.
9. From FV cells that are not visited by streamlines from step 2, a second family of streamlines is launched and steps 3 to 8 are performed (Section 4.4 in [14]). The saturation distributions along streamlines are mapped back to the FV grid cells.
10. Steps 1 to 10 are repeated until the global time steps Δt_g add up to the desired simulation end time.

This algorithm is applicable for cases where constant pressures are prescribed at in- and outflow boundaries. In the case of prescribed total inflow flux boundaries, the algorithm becomes more involved.

3.2. Numerical Buckley-Leverett Solver

For step 7 of the streamline solution algorithm, the Buckley-Leverett equation (11) needs to be solved along streamlines. With only one flow direction along a streamline, a standard upwind solver with explicit Euler time integration (see for example Section 4.8 in [18]) is suitable. However, the injection

step size $\delta Q \leq \Delta Q$ in Q-direction is restricted because of irregularities in the grid cell widths ΔV. These irregularities are caused by varying streamline cell sizes Δr and cross sections $A(r)$. To reduce limitations with respect to small δQ, a regularization step is typically performed [13]. However, regularization is not straight forward and involves interpolation of the water saturation S_w when mapping between regular and irregular grids along the V-coordinate.

In this work, an adaptive regularization method is proposed. Whenever a cell is on the verge of over- or under-flowing, i.e. when the current flux balance and the current ΔV-δQ-ratio lead to $S_w > 1$ or $S_w < 0$, respectively, this cell is merged with its downstream neighbor. In the merging step, the initial cell saturations are volume averaged and the combined cell can handle larger fluxes due to an increased volume ΔV. For a given δQ, the merging procedure is continued until an over- or under-flow is averted.

3.3. Analytical Buckley-Leverett Solver

For a Riemann-type initial saturation S_w, the Buckley-Leverett equation (11) in step 7 has an analytical solution that is derived in AppendixA. In this work, the analytical solution is an option for reservoirs that are initially entirely filled with oil, i.e. $S_w = 0$, and flooded with water, which means that $S_w = 1$ at the inflow boundary (or at $V = 0$). Also, the fixed streamline assumption must hold for the entire simulation time with only intermediate time steps and no global pressure updates being performed. For heterogeneous reservoirs, the fixed streamline assumption is reasonable because the streamline pattern is dominated by variations in k and changes in the relative permeability are less important (page 384 in [5]). Nevertheless, relative permeability effects are accounted for through the streamline resistance R. If global pressure updates are performed, however, the streamline pattern changes and the initial condition for subsequent intermediate time steps disables the use of the analytical Buckley-Leverett solution.

4. Uncertain Permeability Field

In this work, a Gaussian geostatistical model is applied to characterize the uncertain logarithmic permeability $y = \ln(k)$. Random Gaussian fields are determined by a mean and a covariance function. Since MLMC is a sampling-based method, a generator to compute permeability field realizations according to the chosen geostatistical model is needed. In this work, a spectral method relying on FFTs is applied. See AppendixB for details.

5. Multilevel Monte Carlo (MLMC)

In this section, the MLMC framework is introduced. More details about MLMC are available in the works of Giles [8] and Schwab et al. [10, 11]. Even though MLMC is applied in this work to determine the uncertainty of the water saturation S_w, we use u in the following as a generic variable to simplify the notation.

5.1. MLMC Estimator

Let u be the random solution of a stochastic PDE and u_ℓ with $\ell = 1, \ldots, L$ approximations of u resulting from solving a discretized version of the PDE. The index ℓ encodes the accuracy of u_ℓ with respect to the true solution u. As ℓ is increased, the meshing used to discretize the PDE is refined. Consequently, u_L denotes the solution computed on the finest grid. u_L can be written as a telescopic sum in terms of u_ℓ with $\ell = 1, \ldots, L$,

$$u_L = u_L - u_{L-1} + u_{L-1} - u_{L-2} + \ldots = \sum_{\ell=1}^{L} u_\ell - u_{\ell-1},$$

with $u_0 = 0$. In this work, level ℓ refers to the discretization difference $u_\ell - u_{\ell-1}$. Taking the expectation on both sides and recalling its linearity leads to

$$\mathbb{E}[u_L] = \sum_{\ell=1}^{L} \mathbb{E}[u_\ell - u_{\ell-1}]. \tag{13}$$

Let $E_M[.]$ be the ensemble average over M independent and identically distributed samples. The MLMC estimator for the expected value of u_L, $E[u_L]$, is obtained from replacing the expected values on the right hand side by ensemble averages $E_{M_\ell}[.]$,

$$\mathbb{E}[u_L] \approx E[u_L] = \sum_{\ell=1}^{L} E_{M_\ell}[u_\ell - u_{\ell-1}] = \sum_{\ell=1}^{L} \frac{1}{M_\ell} \sum_{i=1}^{M_\ell} (u_\ell^i - u_{\ell-1}^i). \tag{14}$$

Here, $u_\ell^i - u_{\ell-1}^i$ denotes the difference between discretizations ℓ and $\ell - 1$ of realization i. For one particular i, u_ℓ^i and $u_{\ell-1}^i$ on level ℓ are computed based on the same random input realization. In the setting of uncertain permeability, this means that the according k_ℓ^i and $k_{\ell-1}^i$ should be derived from the same permeability realization. Hence, k_ℓ^i and $k_{\ell-1}^i$ on level ℓ differ only in the discretization. On the other hand, random input realizations on different levels are drawn independently from each other. Note also that the number of samples M_ℓ computed for the ensemble average $E_{M_\ell}[.]$ is level dependent.

Starting from a telescopic sum for u_L^q with a positive integer power q, the derivation for the MLMC estimator above extends also to higher moments,

$$\mathbb{E}[u_L^q] \approx E[u_L^q] = \sum_{\ell=1}^{L} E_{M_\ell}[u_\ell^q - u_{\ell-1}^q] = \sum_{\ell=1}^{L} \frac{1}{M_\ell} \sum_{i=1}^{M_\ell} ((u_\ell^i)^q - (u_{\ell-1}^i)^q).$$

It is noted that throughout this paper, the term "higher moment" or more specifically the term "q'th moment" (with q being a positive integer) always refers to $\mathbb{E}[(\cdot)^q]$.

5.2. MLMC Sampling Error

Once the discretization error linked to the finest discretization u_L is accepted, the remaining error of interest is due to sampling. In other words, we are interested in the error introduced by replacing the expected value by the MLMC estimator,

$$\|\mathbb{E}[u_L] - E[u_L]\|_{L^2(\Omega;L^2(D))}, \tag{15}$$

where D denotes the physical domain whose points are described by the Cartesian coordinates $\boldsymbol{x}$. For the test cases studied in this work, time is fixed and D denotes the reservoir domain. However in general, D may span over time as well. In expression (15), Ω denotes the stochastic domain with random event coordinate ω (and corresponding probability measure $d\omega$). The L^2-norm corresponds to either $\sqrt{\int_D (\cdot)^2 d\boldsymbol{x}}$ or $\sqrt{\int_\Omega (\cdot)^2 d\omega}$. The error norm above is therefore to be understood as a sort of root mean square,

$$\|\cdot\|_{L^2(\Omega;L^2(D))} = \sqrt{\int_\Omega \int_D (\cdot)^2 d\boldsymbol{x} d\omega} = \sqrt{\mathbb{E}\left[\int_D (\cdot)^2 d\boldsymbol{x}\right]}.$$

The square of the sampling error (15) can be decomposed as follows,

$$\begin{aligned}
&\|\mathbb{E}[u_L] - E[u_L]\|^2_{L^2(\Omega;L^2(D))} \\
&= \|\mathbb{E}[u_L] - \sum_{\ell=1}^{L} \frac{1}{M_\ell} \sum_{i=1}^{M_\ell} (u_\ell^i - u_{\ell-1}^i)\|^2_{L^2(\Omega;L^2(D))} \\
&= \|\sum_{\ell=1}^{L} \frac{1}{M_\ell} \sum_{i=1}^{M_\ell} \mathbb{E}[u_\ell - u_{\ell-1}] - (u_\ell^i - u_{\ell-1}^i)\|^2_{L^2(\Omega;L^2(D))} \\
&= \mathbb{E}\Big[\int_D \Big(\sum_{\ell=1}^{L} \frac{1}{M_\ell} \sum_{i=1}^{M_\ell} \mathbb{E}[u_\ell - u_{\ell-1}] - (u_\ell^i - u_{\ell-1}^i)\Big) \\
&\qquad \Big(\sum_{k=1}^{L} \frac{1}{M_k} \sum_{j=1}^{M_k} \mathbb{E}[u_k - u_{k-1}] - (u_k^j - u_{k-1}^j)\Big) d\boldsymbol{x}\Big] \\
&= \sum_{\ell=1}^{L}\sum_{k=1}^{L} \frac{1}{M_\ell}\frac{1}{M_k} \sum_{i=1}^{M_\ell}\sum_{j=1}^{M_k} \mathbb{E}\Big[\int_D \Big(\mathbb{E}[u_\ell - u_{\ell-1}] - (u_\ell^i - u_{\ell-1}^i)\Big) \\
&\qquad \Big(\mathbb{E}[u_k - u_{k-1}] - (u_k^j - u_{k-1}^j)\Big) d\boldsymbol{x}\Big].
\end{aligned} \tag{16}$$

Since different samples are mutually independent, terms with $i \neq j$ vanish. Since the sampling on different levels is independent, also terms with $\ell \neq k$

vanish. Hence,

$$\begin{aligned}
&\|\mathbb{E}[u_L] - E[u_L]\|^2_{L^2(\Omega;L^2(D))} \\
&= \sum_{\ell=1}^{L} \frac{1}{M_\ell^2} \sum_{i=1}^{M_\ell} \mathbb{E}\Big[\int_D \Big(\mathbb{E}[u_\ell - u_{\ell-1}] - (u_\ell^i - u_{\ell-1}^i) \Big)^2 d\boldsymbol{x} \Big] \\
&= \sum_{\ell=1}^{L} \frac{1}{M_\ell} \mathbb{E}\Big[\int_D \Big(\mathbb{E}[u_\ell - u_{\ell-1}] - (u_\ell - u_{\ell-1}) \Big)^2 d\boldsymbol{x} \Big] \\
&= \sum_{\ell=1}^{L} \frac{1}{M_\ell} \underbrace{\|\mathbb{E}[u_\ell - u_{\ell-1}] - (u_\ell - u_{\ell-1})\|^2_{L^2(\Omega;L^2(D))}}_{=\sigma_\ell^2} = \sum_{\ell=1}^{L} \frac{\sigma_\ell^2}{M_\ell}, \qquad (17)
\end{aligned}$$

where σ_ℓ^2 denote level variances. In summary, the squared sampling error can be written as a sum of individual level errors.

Compared to a standard MC method, which is based on the single level $u_{L=1} - 0$, MLMC splits the square of the sampling error into several smaller contributions σ_ℓ^2/M_ℓ with $\ell = 1, \ldots, L$. MLMC benefits from the fact that σ_ℓ^2/M_ℓ at coarse levels (with ℓ being small) are reduced efficiently since samples can be calculated at low computational cost and therefore M_ℓ is increased with little effort. At fine levels (with ℓ being large), the level variances σ_ℓ^2 are typically small and thus M_ℓ can be small, which means only few expensive computations.

5.3. Optimization Problem

Besides the level variances σ_ℓ^2, another quantity of interest is the expected work per sample on a certain level w_ℓ, that is the expected time required to compute one sample of $u_\ell - u_{\ell-1}$. Given σ_ℓ^2 and w_ℓ for all levels $\ell = 1, \ldots, L$, an optimization problem is formulated to find the best choice for the number of samples M_ℓ on each level such that the total work is minimized and the sampling error (17) equals a prescribed threshold ϵ. The total work is defined as

$$w_{tot} = \sum_{\ell=1}^{L} M_\ell w_\ell.$$

The optimization problem is stated by

$$\text{minimize } \sum_{\ell=1}^{L} M_\ell w_\ell \text{ such that } \epsilon^2 = \sum_{\ell=1}^{L} \frac{\sigma_\ell^2}{M_\ell}. \qquad (18)$$

The optimal choice of M_ℓ is given by

$$M_{\ell,opt} = \frac{1}{\epsilon^2} \sqrt{\frac{\sigma_\ell^2}{w_\ell}} \sum_{k=1}^{L} \sigma_k \sqrt{w_k}, \qquad (19)$$

(see also equation (12) in [8]). It is pointed out that the resulting $M_{\ell,opt}$ are not integers and need to be rounded. Moreover, in our case, only estimates for σ_ℓ^2

and w_ℓ are available, i.e., $\tilde{\sigma}_\ell^2$ and $\tilde{w}_\ell$, respectively. These estimates can be computed based on the same samples already involved in the MLMC estimator (14). For example, the individual level variances σ_ℓ^2 can be estimated by

$$\begin{aligned}\sigma_\ell^2 &\approx \tilde{\sigma}_\ell^2 \\ &= \frac{1}{M_\ell - 1}\sum_{j=1}^{M_\ell}\int_D \Big(\frac{1}{M_\ell}\sum_{i=1}^{M_\ell}(u_\ell^i - u_{\ell-1}^i) - (u_\ell^j - u_{\ell-1}^j)\Big)^2 d\boldsymbol{x} \\ &= \frac{1}{M_\ell - 1}\sum_{j=1}^{M_\ell}\left\|\frac{1}{M_\ell}\sum_{i=1}^{M_\ell}(u_\ell^i - u_{\ell-1}^i) - (u_\ell^j - u_{\ell-1}^j)\right\|_{L^2(D)}^2 .\end{aligned}$$

For realizations u_ℓ^i that are represented by a set of cell-wise averaged values, it is straight forward to compute the integral involved in the L^2-norm.

5.4. MLMC Algorithm

In this work, the following MLMC algorithm based on Section 5 of [8] is applied.

1. Fix a sequence of discretizations/grid resolutions $\ell = 1, \ldots, L$; fix a number of warm-up samples M_{up}; fix a threshold ϵ for the estimated sampling error (see equation (18)).
2. Warm-up phase: compute $M_\ell = M_{up}$ samples of $u_\ell - u_{\ell-1}$ on every level.
3. Update the estimates for $E_{M_\ell}[u_\ell - u_{\ell-1}]$, $\tilde{\sigma}_\ell^2$ and $\tilde{w}_\ell$ on every level.
4. Solve the optimization problem (equation (19)) with respect to $\tilde{\sigma}_\ell^2$ and $\tilde{w}_\ell$ and update the required number of samples M_ℓ.
5. For each level ℓ, if the updated M_ℓ is beyond the number of samples already computed, add one sample of $u_\ell - u_{\ell-1}$ and continue with step 3. If no level needs an additional sample, quit.

The choice of warm-up samples M_{up} is somewhat delicate. It should be large enough to determine especially $\tilde{\sigma}_\ell^2$ accurately. On the other hand, if M_{up} is larger than any M_ℓ suggested by the optimization problem in step 4, unnecessary samples are calculated and computation time is wasted.

For higher moments, the MLMC algorithm is analogous.

5.5. Requirements for Random Field Generator

In case of oil water transport in random heterogeneous porous media, MLMC requires permeability realizations to be computed on FV grids with different resolutions. In order to efficiently use MLMC, the generation of permeability fields should (i) be cheaper on coarse grids compared to fine grids. Also, the permeability realizations k_ℓ^i and $k_{\ell-1}^i$ of the same level need to (ii) be dependent, i.e. k_ℓ^i and $k_{\ell-1}^i$ are supposed to be derived from the same realization but discretized on consecutive grids. Otherwise, the corresponding σ_ℓ^2 becomes large. Moreover, the discretized permeability field k_ℓ appears on two consecutive levels. For example, levels $\ell+1$ $(u_{\ell+1} - u_\ell)$ and ℓ $(u_\ell - u_{\ell-1})$ share the discretization ℓ

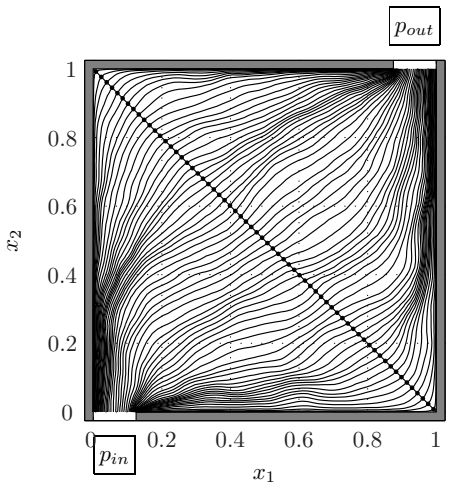

Figure 1: Oil reservoir boundary conditions: grey shaded regions represent no flow boundary conditions and white gaps correspond to the inflow pressure boundary (lower left corner, $p_{in} = 1$) and outflow pressure boundary (top right corner, $p_{out} = 0$). Exemplary streamlines with launch points on the diagonal.

(u_ℓ). The telescopic approach inherent to MLMC requires (iii) that the samples k_ℓ^i on both levels share the same statistics. Otherwise, $\mathbb{E}[u_\ell]$ on successive levels become unequal and the telescopic equality (13) becomes invalid.

The permeability realizations k_ℓ^i are computed from their logarithmic counterparts y_ℓ^i through $k_\ell^i = \exp(y_\ell^i)$. Permeability realizations within a level are generated as follows. Assuming the mean and covariance of $y_{\ell+1}$ are known, a realization $y_{\ell+1}^i$ can be computed on level $\ell + 1$ using the spectral field generator described in AppendixB. The field y_ℓ^i on the same level is derived from cell averaging $y_{\ell+1}^i$ (see equation (C.1) in AppendixC and figure 2). Cell averaging honors requirement (ii). According to requirement (iii), the realizations y_ℓ^i on level ℓ need to have the same statistical characterization as the realizations y_ℓ^i resulting from cell averaging on level $\ell + 1$. Based on the process $y_{\ell+1}$ on level $\ell + 1$ and the cell averaging procedure involved, it is possible to compute the discrete covariance function or covariance matrix of process y_ℓ on level ℓ such that requirement (iii) is fulfilled. Details about this are provided in AppendixC. With the covariance of y_ℓ on level ℓ at hand, also requirement (i) is fulfilled, since realizations y_ℓ^i on level ℓ can be generated directly with the required grid resolution.

6. Test Cases

A two dimensional, initially saturated oil reservoir, i.e. $S_w(\boldsymbol{x}, t = 0) = 0$, is considered to numerically demonstrate the applicability of the MLMC technique. The oil reservoir depicted in figure 1 is quadratic with side length 1 and is subject to water injection in the left lower corner with pressure $p = 1$ and

	standard deviation σ_y	correlation length η_y
test case 1	1	0.4
test case 2	1	0.2
test case 3	2	0.4
test case 4	2	0.2

Table 1: Test cases.

	MLMC or MC	fixed streamline assumption	Buckley-Leverett solver
run 1	MLMC	yes	analytical
run 2	MC	yes	analytical
run 3	MLMC	no	numerical
run 4	MC	no	numerical
run 5	MC	yes	numerical

Table 2: Runs.

water saturation $S_w = 1$ and extraction in the top right corner at a pressure $p = 0$. Besides pressure in- and outflow boundaries, the reservoir is confined. The viscosities of water and oil are set to $\mu_w = 1$ and $\mu_o = 10$, respectively, and the porosity is set to $\phi = 1$. A quadratic relative permeability model is chosen, i.e. $k_{r,w} = S_w^2$ for the water phase and $k_{r,o} = (1 - S_w)^2$ for oil.

The logarithmic permeability $y = \ln(k)$ is modeled with a random Gaussian field. This process is defined by the mean $\bar{y}$ and the covariance $C_y(\boldsymbol{x}, \boldsymbol{x}')$ at locations $\boldsymbol{x} = [x_1, x_2]^\top$ and $\boldsymbol{x}' = [x_1', x_2']^\top$. A stationary spatial exponential covariance function is chosen, i.e.

$$C_y(\boldsymbol{x}, \boldsymbol{x}') = \sigma_y^2 \exp\left(-\frac{1}{\eta_y}\sqrt{(x_1 - x_1')^2 + (x_2 - x_2')^2}\right),$$

where σ_y denotes the standard deviation of y and η_y the correlation length. Since the covariance is stationary in space, $C_y(\boldsymbol{x}, \boldsymbol{x}')$ depends no longer on the two different locations $\boldsymbol{x}$ and $\boldsymbol{x}'$, but only on their separation vector, i.e. $C_y(\boldsymbol{x}, \boldsymbol{x}') = C_y(|\boldsymbol{x} - \boldsymbol{x}'|)$. Test cases with $\sigma_y = 1, 2$ and $\eta_y = 0.2, 0.4$ are considered and summarized in table 1. The mean of the logarithmic permeability is set to $\bar{y} = 0$.

For the indicated correlation lengths and variances of the logarithmic permeability field, the first moment estimate of the water saturation S_w at time $t_{end} = 10$ is calculated by MLMC and MC according to the runs listed in table 2. Runs 1 and 2 enable a comparison of MLMC and MC in case of fixed streamlines and an analytical Buckley-Leverett solver (see Section 3). A similar comparison can be made based on runs 3 and 4 without the fixed streamline assumption such that global pressure updates are performed and a numerical Buckley-Leverett solver is required. Moreover, the impact of the fixed streamline assumption and the performance of the numerical Buckley-Leverett solver are investigated by comparing runs 4 and 5, and runs 2 and 5, respectively.

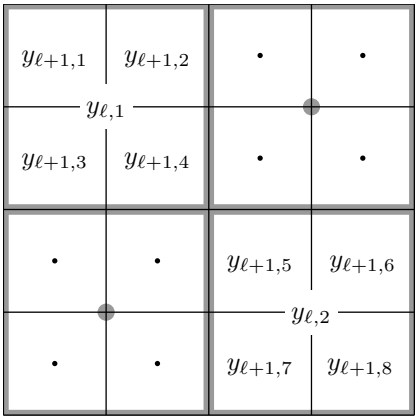

Figure 2: Grid cells and cell centers of consecutive discretizations ℓ (coarse, bold gray) and $\ell + 1$ (fine, regular black). Exemplary logarithmic permeabilities y_ℓ (coarse) and $y_{\ell+1}$ (fine).

7. Numerical Method

In this section, details about the numerical implementation of the two phase transport, streamline-based, MLMC framework are provided.

The FV grid used to discretize the reservoir domain is regular and Cartesian. The grids of different disrcretizations are nested and aligned with respect to the cell interfaces (see figure 2).

Computing realizations of level differences, i.e. $S^i_{w,\ell} - S^i_{w,\ell-1}$ at time $t_{end} = 10$, which are part of the MLMC estimator (see equation (14)), is straight forward since cell constant values are assumed.

In step 2 of the streamline algorithm presented in Section 3.1, Pollock's algorithm [17] is used to generate streamlines based on $\boldsymbol{q}_{tot}$. The streamlines resulting from forward and backward tracking originate from uniformly distributed launch points on the diagonal of the square domain as seen in figure 1.

Details on the implementation of the analytical Buckley-Leverett solver are provided at the end of AppendixA.

7.1. MLMC Parameters and Discretization

It is outlined in Section 5.1 that a MLMC simulation involves several levels $\ell = 1, \ldots, L$, where each level ℓ is associated with a difference of discretizations ℓ and $\ell - 1$. In the present context, the term discretization does not only refer to the FV grid used to solve for the global pressure. It involves additional parameters like the number of streamlines, the number of transport steps, and others, all of which are listed in table 3. The discretization $\ell = 0$ is called the null discretization with $u_0 = 0$ or more specifically $S_{w,\ell=0} = 0$. The MLMC discretization parameters are changed for different runs (listed in table 2) but are the same for the different test cases (listed in table 1).

In the following, the variations of MLMC discretization parameters for the different runs are documented. Given the number of levels L, the coarsest

N_1, N_2	number of FV grid cells in x_1 and x_2 directions
N_{sl}	number of streamlines
$N_{\Delta t_g}$	number of time steps for global pressure updates
$N_{\Delta t_i}$	number of intermediate time steps for transport on streamlines
$N_{\delta Q}$	number of injection steps for numerical Buckley-Leverett solver (see also Section 3.2)
N_ξ	number of entries in the look-up table for the analytical Buckley-Leverett solver (see also AppendixA)

Table 3: MLMC discretization parameters.

value of a discretization parameter and a refinement factor, the parameters' changes from discretization to discretization are fully determined. For example, by setting the number of levels L to 5, the coarsest number of streamlines to 8 and its refinement factor to 2 results in a sequence of $N_{sl} = 8 \cdot 2^{\ell-1}$ streamlines for the discretizations $\ell = 1, \ldots, 5$. In case of the null discretization, i.e. $\ell = 0$, no grid is required.

Run 1 is a MLMC simulation based on the fixed streamline assumption with MLMC parameters included in table 4. With no global pressure updates being made, $N_{\Delta t_g} = 1$. Since the analytical Buckley-Leverett solver is applied, the number of look-up table entries N_ξ is relevant.

Run 2 is a MC simulation based on the fixed streamline assumption and the analytical Buckley-Leverett solver. The discretization parameters for run 2 are given in table 5. As mentioned at the end of Section 5.2, MC can be interpreted as MLMC with just one level, i.e. $L = 1$ and its only non null discretization is the coarsest and the finest discretization simultaneously. In order to compare MLMC and MC, the finest discretizations of run 1 and run 2 are equal. Since $L = 1$, refinement factors do not apply.

Run 3 is a MLMC simulation with global pressure updates. Hence in general $N_{\Delta t_g} > 1$, the numerical Buckley-Leverett solver is applied and N_ξ becomes irrelevant. The discretization parameters for run 3 are provided in table 6. We point out that the total number of intermediate updates for the MLMC runs 1 and 3 are equal for every discretization, i.e. $N_{\Delta t_g} N_{\Delta t_i} = 2$ ($\ell = 1$), 4 ($\ell = 2$), $\ldots$, 32 ($\ell = L = 5$). In addition, the number of injection steps δQ for the numerical Buckley-Leverett solver, i.e. $N_{\delta Q} = 4$, leads to a further division in time.

Run 4 is the MC counterpart of MLMC run 3. Again, this simulation involves $L = 1$ level and its only non null discretization matches the finest discretization of run 3. Moreover, the total number of intermediate updates of the MC runs 2 and 4 are equal, i.e. 32. The discretization parameters for run 4 are given in table 7.

Run 5 is a MC simulation based on the fixed streamline assumption. However, for validation purposes a numerical Buckley-Leverett solver is used. This run is mainly included to investigate the influence of the fixed streamline assumption. The discretization parameters are the same as for run 2 with $N_{\delta Q} = 4$

	coarsest discretization	finest discretization	refinement factor	L
N_1	8	128	2	
N_2	8	128	2	
N_{sl}	8	128	2	
$N_{\Delta t_g}$	1	1	1	5
$N_{\Delta t_i}$	2	32	2	
$N_{\delta Q}$	-	-	-	
N_ξ	8	128	2	

Table 4: MLMC discretization parameters. Run 1: MLMC, fixed streamlines, analytical Buckley-Leverett solver.

	coarsest discretization	finest discretization	refinement factor	L
N_1	128	128	-	
N_2	128	128	-	
N_{sl}	128	128	-	
$N_{\Delta t_g}$	1	1	-	1
$N_{\Delta t_i}$	32	32	-	
$N_{\delta Q}$	-	-	-	
N_ξ	128	128	-	

Table 5: MLMC discretization parameters. Run 2: MC, fixed streamlines, analytical Buckley-Leverett solver.

added. The discretization parameters for run 5 are listed in table 8.

Each set of MLMC parameters defines the finest discretization L. This finest discretization should sufficiently resolve the flow and transport processes under consideration. The L^2-norm of the estimated discretization difference $\|E_{M_L}[S_{w,L} - S_{w,L-1}]\|_{L^2(D)}$ is an indicator for the accuracy at the finest discretization L. For the most challenging test case 4 (in terms of resolution in space and time), $\|E_{M_L}[S_{w,L} - S_{w,L-1}]\|_{L^2(D)} = 0.008$ at time $t_{end} = 10$ for the MLMC runs 1 and 3, which is considered to be sufficiently small. More sophisticated MLMC algorithms could add finer levels, if $\|E_{M_L}[S_{w,L} - S_{w,L-1}]\|_{L^2(D)}$ is above a certain threshold. Other choices of MLMC discretization parameters

	coarsest discretization	finest discretization	refinement factor	L
N_1	8	128	2	
N_2	8	128	2	
N_{sl}	8	128	2	
$N_{\Delta t_g}$	1	16	2	5
$N_{\Delta t_i}$	2	2	1	
$N_{\delta Q}$	4	4	1	
N_ξ	-	-	-	

Table 6: MLMC discretization parameters. Run 3: MLMC, no fixed streamlines, numerical Buckley-Leverett solver.

	coarsest discretization	finest discretization	refinement factor	L
N_1	128	128	-	
N_2	128	128	-	
N_{sl}	128	128	-	
$N_{\Delta t_g}$	16	16	-	1
$N_{\Delta t_i}$	2	2	-	
$N_{\delta Q}$	4	4	-	
N_{ξ}	-	-	-	

Table 7: MLMC discretization parameters. Run 4: MC, no fixed streamlines, numerical Buckley-Leverett solver.

	coarsest discretization	finest discretization	refinement factor	L
N_1	128	128	-	
N_2	128	128	-	
N_{sl}	128	128	-	
$N_{\Delta t_g}$	1	1	-	1
$N_{\Delta t_i}$	32	32	-	
$N_{\delta Q}$	4	4	-	
N_{ξ}	-	-	-	

Table 8: MLMC discretization parameters. Run 5: MC, fixed streamlines, numerical Buckley-Leverett solver.

and refinement factors are conceivable but the current sets prove to be suitable in the present work.

Finally, additional parameters for the MLMC algorithm (Section 5.4) are provided. The threshold for the estimated sampling error is set to $\epsilon = 0.003$ and the number of warm-up samples is set to $M_{up} = 100$. This choice provides reasonable first estimates for the variance $\tilde{\sigma}_\ell^2$ and the work per sample $\tilde{w}_\ell$ on each level. Moreover, in all simulations performed $M_{up} < M_\ell$ on all levels ℓ and therefore no unnecessary samples are generated.

8. Results and Discussion

In this section, different comparisons are conducted for the four test cases listed in table 1. In the first comparison, i.e. comparison 1, MLMC and MC implementations with the fixed streamline assumption (runs 1 and 2 in table 2) are used. In comparison 2, MLMC and MC implementations with global pressure updates (no fixed streamlines, runs 3 and 4) are applied. Comparisons 1 and 2 are used to investigate the performance gain of MLMC compared to MC. For comparison 1, the finest discretizations of the MLMC run 1 and the MC run 2 agree as well as the thresholds for the estimated sampling error ϵ. Therefore, the MLMC run 1 and the MC run 2 produce results of equal quality. The same holds true for comparison 2. Comparison 3 is about the accuracy of the numerical Buckley-Leverett solver (runs 2 and 5) and the applicability of the

		test case 1 $\sigma_y = 1$ $\eta_y = 0.4$	test case 2 $\sigma_y = 1$ $\eta_y = 0.2$	test case 3 $\sigma_y = 2$ $\eta_y = 0.4$	test case 4 $\sigma_y = 2$ $\eta_y = 0.2$
comparison 1 (fixed streamlines)	run 1 (MLMC): CPU time run 2 (MC): CPU time run 1 vs. run 2: speedup figure reference	2.6 min 18.5 min 7.1 3	3.3 min 16.9 min 5.2 4	4.3 min 49.5 min 11.5 5	6.6 min 50.5 min 7.6 6
comparison 2 (no fixed streamlines)	run 3 (MLMC): CPU time run 4 (MC): CPU time run 3 vs. run 4: speedup figure reference	15.8 min 2.9 h 11.2 7	21.3 min 2.8 h 7.9 8	24.8 min 7.7 h 18.7 9	37.8 min 7.7 h 12.2 10
comparison 3	$\|E_{run_2}[S_w] - E_{run_5}[S_w]\|_{L^2(D)}$ $\|E_{run_4}[S_w] - E_{run_5}[S_w]\|_{L^2(D)}$ figure reference	0.0018 0.0159 11	0.0017 0.0183 11	0.0022 0.0137 11	0.0020 0.0173 11

Table 9: Summary of numerical results.

fixed streamline assumption (runs 4 and 5). To this end, L^2-norms, for example $\|E_{run_2}[S_w] - E_{run_5}[S_w]\|_{L^2(D)}$, are evaluated at time $t_{end} = 10$. The results for the three comparisons and the four test cases are summarized in table 9.

For comparisons 1 and 2, first moment estimates of the water saturation at time $t_{end} = 10$ of MLMC (runs 1 and 2) and MC computations (runs 3 and 4) are shown in figures 3 (a) to 6 (a) and 7 (a) to 10 (a) for test cases 1 to 4. In the panels (b) of these figures, level-dependent quantities are provided, i.e. standard deviation estimates $\tilde{\sigma}_\ell$, estimates for the expected work per sample $\tilde{w}_\ell$ and the number of samples computed M_ℓ. Since MC runs 2 and 4 involve one level only, the corresponding $\tilde{\sigma}_1$, $\tilde{w}_1$ and M_1 are depicted as straight horizontal lines.

In equation (17), the sampling error is decomposed in terms of the standard deviations σ_ℓ and the number of samples M_ℓ. By inspection of figures 3(b) to 10(b) it becomes clear that the estimated $\tilde{\sigma}_\ell$ and the estimated work per sample $\tilde{w}_\ell$ are in advantage of MLMC. The work per sample is small for levels with coarse discretizations and high $\tilde{\sigma}_\ell$, whereas the converse holds true for levels with fine discretizations (ℓ is large). This is the basis for MLMC being faster than MC. The particular numbers of samples M_ℓ (determined by the optimization problem outlined in Section 5.3) are also plotted in figures 3(b) to 10(b).

The fixed streamline assumption has an influence on the MLMC-MC speedup factor. In general, the growth in $\tilde{w}_\ell$ for increasing ℓ is more pronounced if the fixed streamline assumption and the analytical Buckley-Leverett solver are dropped in favor of global pressure updates (compare $\tilde{w}_\ell$ for example in figures 3(b) and 7(b)). As seen in table 9 when comparing the speedup factors of MLMC with respect to MC between comparisons 1 (with fixed streamlines) and 2 (without fixed streamlines), a larger growth in $\tilde{w}_\ell$ is advantageous for MLMC.

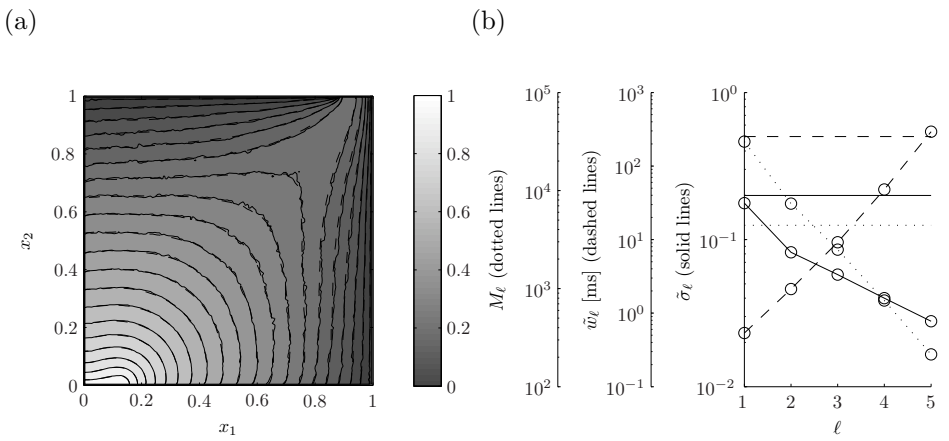

Figure 3: Test case 1: $\sigma_y = 1$, $\eta_y = 0.4$. Comparison 1: run 1 (MLMC) vs. run 2 (MC), fixed streamlines, analytical Buckley-Leverett solver. (a) first moment of S_w at time $t_{end} = 10$: run 1 (solid lines) vs. run 2 (dashed lines). (b) level standard deviation estimates $\tilde{\sigma}_\ell$ (solid lines), level expected work estimates $\tilde{w}_\ell$ (dashed lines), level number of samples M_ℓ (dotted lines): run 1 (curves with different values for levels ℓ) vs. run 2 (horizontal lines).

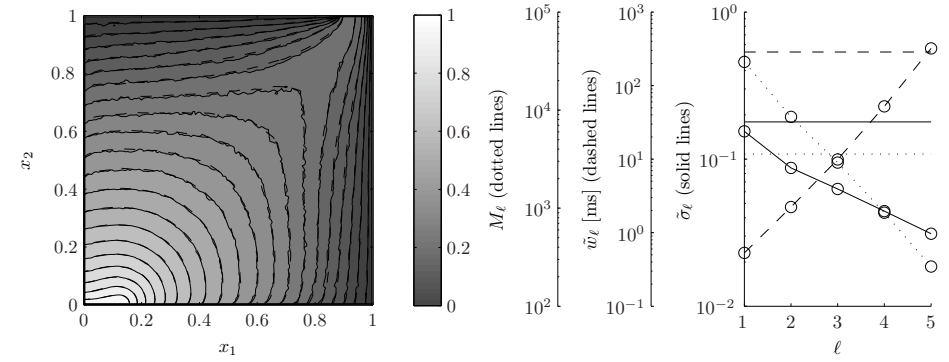

Figure 4: Test case 2: $\sigma_y = 1$, $\eta_y = 0.2$. Comparison 1: run 1 (MLMC) vs. run 2 (MC), fixed streamlines, analytical Buckley-Leverett solver. (a) first moment of S_w at time $t_{end} = 10$: run 1 (solid lines) vs. run 2 (dashed lines). (b) level standard deviation estimates $\tilde{\sigma}_\ell$ (solid lines), level expected work estimates $\tilde{w}_\ell$ (dashed lines), level number of samples M_ℓ (dotted lines): run 1 (curves with different values for levels ℓ) vs. run 2 (horizontal lines).

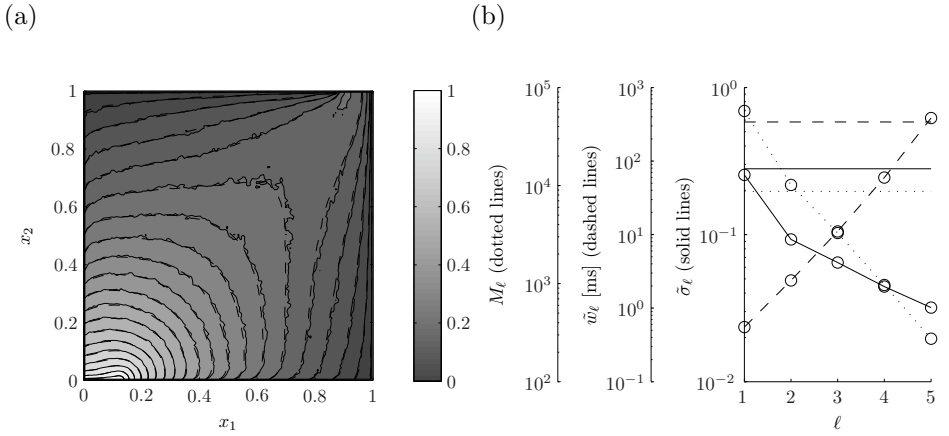

Figure 5: Test case 3: $\sigma_y = 2$, $\eta_y = 0.4$. Comparison 1: run 1 (MLMC) vs. run 2 (MC), fixed streamlines, analytical Buckley-Leverett solver. (a) first moment of S_w at time $t_{end} = 10$: run 1 (solid lines) vs. run 2 (dashed lines). (b) level standard deviation estimates $\tilde{\sigma}_\ell$ (solid lines), level expected work estimates $\tilde{w}_\ell$ (dashed lines), level number of samples M_ℓ (dotted lines): run 1 (curves with different values for levels ℓ) vs. run 2 (horizontal lines).

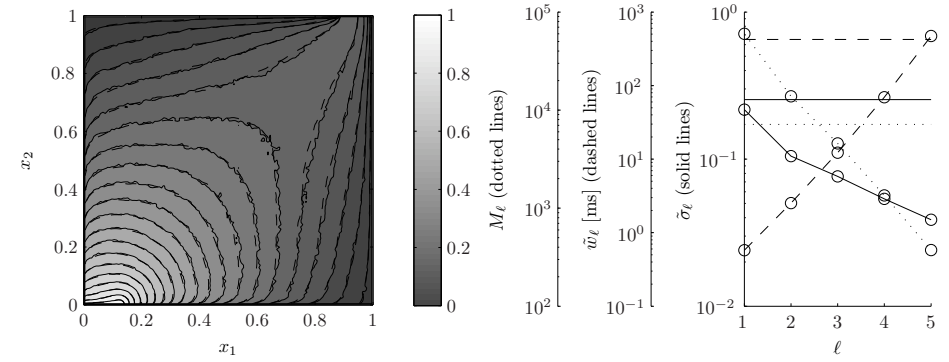

Figure 6: Test case 4: $\sigma_y = 2$, $\eta_y = 0.2$. Comparison 1: run 1 (MLMC) vs. run 2 (MC), fixed streamlines, analytical Buckley-Leverett solver. (a) first moment of S_w at time $t_{end} = 10$: run 1 (solid lines) vs. run 2 (dashed lines). (b) level standard deviation estimates $\tilde{\sigma}_\ell$ (solid lines), level expected work estimates $\tilde{w}_\ell$ (dashed lines), level number of samples M_ℓ (dotted lines): run 1 (curves with different values for levels ℓ) vs. run 2 (horizontal lines).

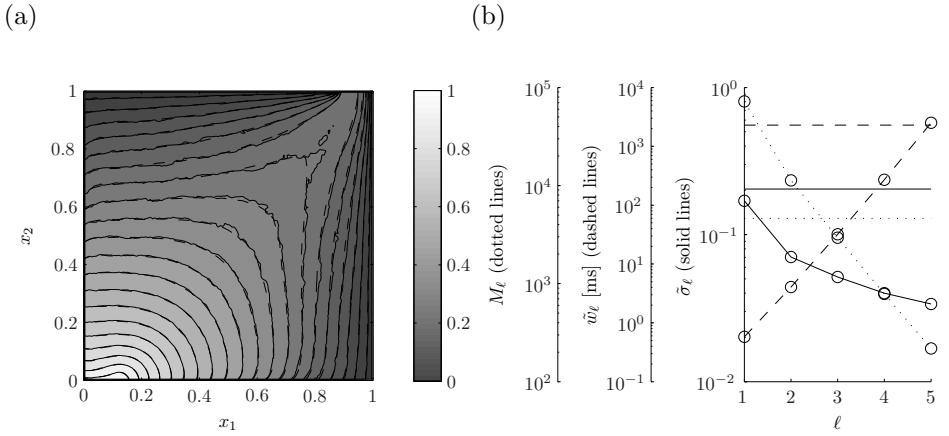

Figure 7: Test case 1: $\sigma_y = 1$, $\eta_y = 0.4$. Comparison 2: run 3 (MLMC) vs. run 4 (MC), no fixed streamlines, numerical Buckley-Leverett solver. (a) first moment of S_w at time $t_{end} = 10$: run 3 (solid lines) vs. run 4 (dashed lines). (b) level standard deviation estimates $\tilde{\sigma}_\ell$ (solid lines), level expected work estimates $\tilde{w}_\ell$ (dashed lines), level number of samples M_ℓ (dotted lines): run 3 (curves with different values for levels ℓ) vs. run 4 (horizontal lines).

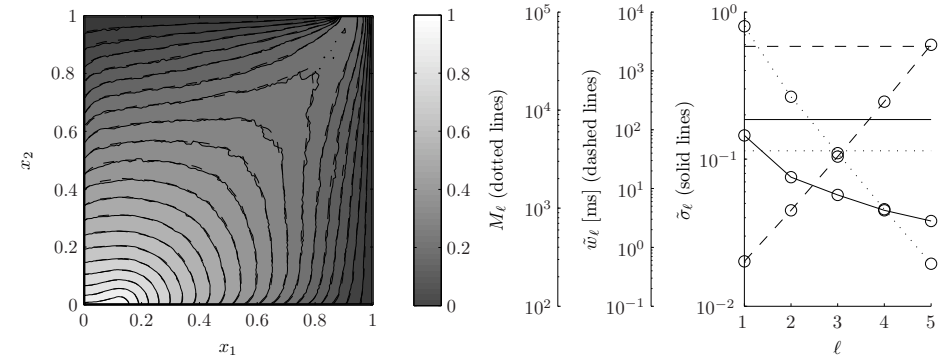

Figure 8: Test case 2: $\sigma_y = 1$, $\eta_y = 0.2$. Comparison 2: run 3 (MLMC) vs. run 4 (MC), no fixed streamlines, numerical Buckley-Leverett solver. (a) first moment of S_w at time $t_{end} = 10$: run 3 (solid lines) vs. run 4 (dashed lines). (b) level standard deviation estimates $\tilde{\sigma}_\ell$ (solid lines), level expected work estimates $\tilde{w}_\ell$ (dashed lines), level number of samples M_ℓ (dotted lines): run 3 (curves with different values for levels ℓ) vs. run 4 (horizontal lines).

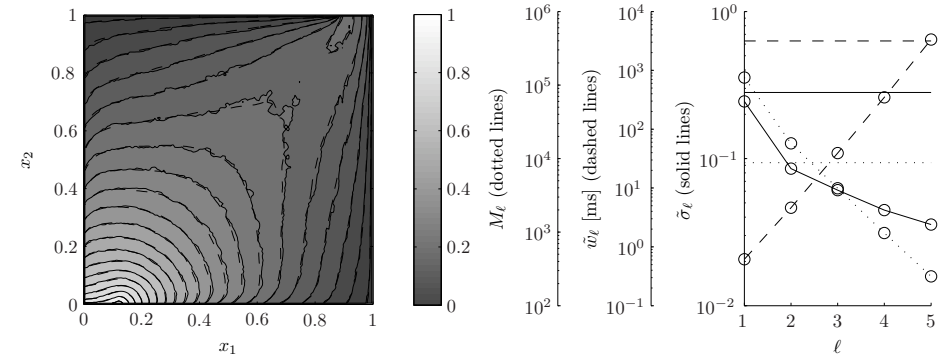

Figure 9: Test case 3: $\sigma_y = 2$, $\eta_y = 0.4$. Comparison 2: run 3 (MLMC) vs. run 4 (MC), no fixed streamlines, numerical Buckley-Leverett solver. (a) first moment of S_w at time $t_{end} = 10$: run 3 (solid lines) vs. run 4 (dashed lines). (b) level standard deviation estimates $\tilde{\sigma}_\ell$ (solid lines), level expected work estimates $\tilde{w}_\ell$ (dashed lines), level number of samples M_ℓ (dotted lines): run 3 (curves with different values for levels ℓ) vs. run 4 (horizontal lines).

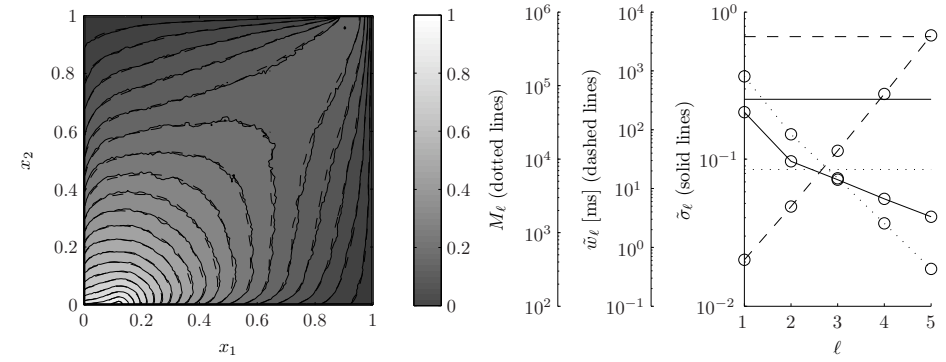

Figure 10: Test case 4: $\sigma_y = 2$, $\eta_y = 0.2$. Comparison 2: run 3 (MLMC) vs. run 4 (MC), no fixed streamlines, numerical Buckley-Leverett solver. (a) first moment of S_w at time $t_{end} = 10$: run 3 (solid lines) vs. run 4 (dashed lines). (b) level standard deviation estimates $\tilde{\sigma}_\ell$ (solid lines), level expected work estimates $\tilde{w}_\ell$ (dashed lines), level number of samples M_ℓ (dotted lines): run 3 (curves with different values for levels ℓ) vs. run 4 (horizontal lines).

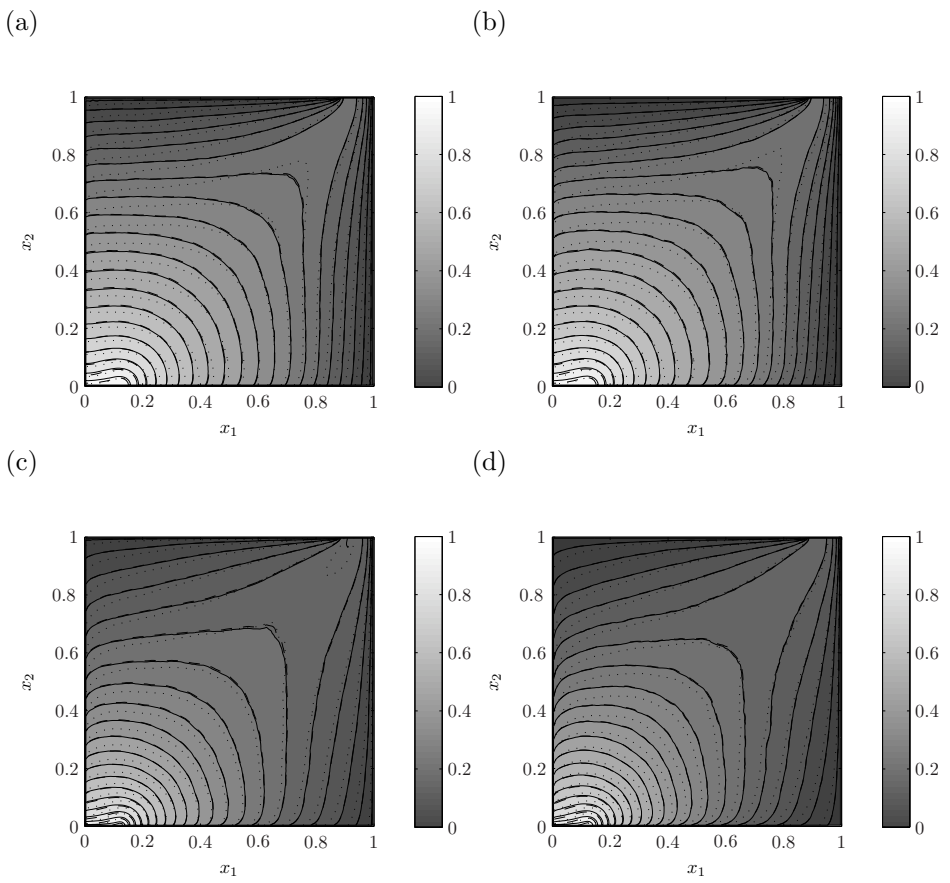

Figure 11: Comparison 3: first moment of S_w at time $t_{end} = 10$ resulting from MC runs 2, 4 and 5. Run 2 (solid lines): fixed streamlines, analytical Buckley-Leverett solver. Run 5 (dashed lines): fixed streamlines, numerical Buckley-Leverett solver. Run 4 (dotted lines): no fixed streamlines, numerical Buckley-Leverett solver. (a) test case 1: $\sigma_y = 1$, $\eta_y = 0.4$. (b) test case 2: $\sigma_y = 1$, $\eta_y = 0.2$. (c) test case 3: $\sigma_y = 2$, $\eta_y = 0.4$. (d) test case 4: $\sigma_y = 2$, $\eta_y = 0.2$.

The MLMC discretization parameters are equal for all test cases with different permeability variability σ_y and correlation lengths η_y. However, the MLMC performance relative to MC varies substantially for the different test cases as seen in table 9.

A key observation is that the MLMC performance with respect to MC suffers from a decrease in the logarithmic permeability correlation length η_y. This is reflected by reductions of MLMC speedups by going from test cases 1 to 2 and from test cases 3 to 4 (see table 9). In case of small η_y, MLMC has to account for more variability in $S_w(t_{end})$ at fine levels with high w_l. Moreover, the coarsest MLMC discretizations may be weakly connected to processes at finer discretizations and consequently coarse discretizations can become hindering in terms of performance. For the test cases with $\eta_y = 0.2$, discarding the coarsest discretization $\ell = 1$ might lead to an improvement. On the other hand, when reducing η_y, the performance of MLMC with respect to MC may be upheld if the discretizations on all levels including the coarsest one are refined accordingly.

As seen in table 9, an increase in σ_y enhances the MLMC performance compared to MC. The MLMC-MC speedup factors increase when going from test cases 1 to 3 and from cases 2 to 4. This is because in contrary to MC where only one level is available, MLMC absorbs most of the additional $S_w(t_{end})$ variability on coarse levels where sampling is cheap. This can be seen for example by comparing figure 3 with 5, and figure 4 with 6.

In comparison 3, the numerical Buckley-Leverett solver is validated and the applicability of the fixed streamline assumption is tested for test cases 1 to 4. In all test cases, the errors listed in table 9 due to the numerical streamline solver, i.e. $\|E_{run_2}[S_w] - E_{run_5}[S_w]\|_{L^2(D)}$ at time $t_{end} = 10$, are substantially smaller than the errors due to the fixed streamline assumption measured by $\|E_{run_4}[S_w] - E_{run_5}[S_w]\|_{L^2(D)}$ at time $t_{end} = 10$. Furthermore, as is also visible in figure 11, an increase in permeability variability σ_y reduces the error due to the fixed streamline assumption. This observation is consistent with the discussion from Section 3.3, where it is claimed that the fixed streamline assumption is reasonable for highly heterogeneous reservoirs. Comparisons 1 and 2 document that the computational costs can be greatly reduced, if the fixed streamline assumption together with the analytical Buckley-Leverett solver is applied and no global pressure updates are performed.

Since in MLMC much fewer samples are computed on the finest discretization compared to MC, the first moment estimates resulting from MLMC are more fine grained. Nevertheless, the estimated sampling errors are equal in MLMC and MC with threshold ϵ set equal. From the definition of the sampling error $\|\mathbb{E}[u_L] - E[u_L]\|_{L^2(\Omega;L^2(D))}$ it is clear that a single difference between $\mathbb{E}[u_L]$ and one particular estimate $E[u_L]$ is not very representative. Despite that, figure 12 is included to demonstrate that a fine grained MLMC solution is not necessarily less accurate than the one by MC. In figure 12, MLMC run 1 and MC run 2 for test case 1 are revisited. First moment estimates of the MLMC run 1 and MC run 2 are shown alongside a reference for $\mathbb{E}[S_w]$ at time $t_{end} = 10$, built from 160 MC runs.

Due to the fact that only ensemble-based estimates of the level variances $\tilde{\sigma}_\ell^2$

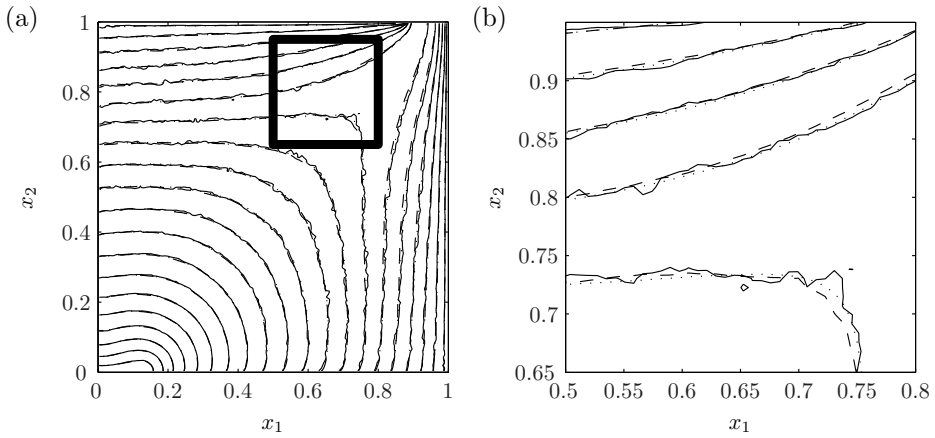

Figure 12: Test case 1, MLMC run 1 (solid line) vs. MC run 2 (dashed line) vs. MC reference (dotted line). (a) first moment of S_w at time $t_{end} = 10$: entire domain. (b) detail indicated by the thick rectangle in (a).

are available, the MLMC algorithm outlined in Section 5.4 can only approximate the prescribed sampling error. Moreover, since $\tilde{\sigma}_\ell^2$ and $\tilde{w}_\ell$ are estimates, they need to be considered random quantities. The numbers of samples M_ℓ depend on $\tilde{\sigma}_\ell^2$ and $\tilde{w}_\ell$ (see optimization problem from Section 5.3) and become random quantities as well. Consequently in the strict sense, interchanging expectation and summation over $i = 1, \ldots, M_\ell$ and $j = 1, \ldots, M_k$ in equation (16) is no longer feasible. However, it is possible to verify the resulting sampling error based on the approximation

$$\begin{aligned}
&\|\mathbb{E}[u_L] - E[u_L]\|_{L^2(\Omega;L^2(D))} \\
&\quad\approx \left(\frac{1}{K-1} \sum_{j=1}^{K} \int_D \left(\left(\frac{1}{K} \sum_{i=1}^{K} E[u_L]^i \right) - E[u_L]^j \right)^2 d\boldsymbol{x} \right)^{1/2} \\
&\quad= \left(\frac{1}{K-1} \sum_{j=1}^{K} \left\| \left(\frac{1}{K} \sum_{i=1}^{K} E[u_L]^i \right) - E[u_L]^j \right\|_{L^2(D)}^2 \right)^{1/2},
\end{aligned}$$

where $E[u_L]^i$ or $E[u_L]^j$ represent outcomes from K independent MLMC simulations. A sampling error of 0.00301 is for example calculated for test case 1 and MLMC run 1 with sampling error threshold $\epsilon = 0.003$ and $K = 160$. Therefore it can be concluded that despite the false assumptions of $\tilde{\sigma}_\ell^2$ being exact and of M_ℓ being deterministic, the MLMC algorithm closely approximates the sampling error.

At the end of Section 5.4, it is claimed that the MLMC framework can also be applied to calculate higher moments. For example in figure 13, the second moment of S_w at time $t_{end} = 10$ is plotted for case 1 with MLMC run 1.

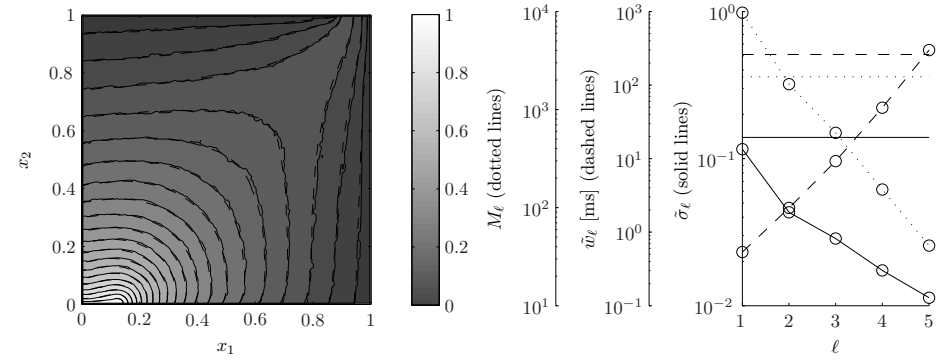

Figure 13: Test case 1: $\sigma_y = 1$, $\eta_y = 0.4$. Comparison 1: run 1 (MLMC) vs. run 2 (MC), fixed streamlines, analytical Buckley-Leverett solver. (a) second moment of S_w at time $t_{end} = 10$: run 1 (solid lines) vs. run 2 (dashed lines). (b) level standard deviation estimates $\tilde{\sigma}_\ell$ (solid lines), level expected work estimates $\tilde{w}_\ell$ (dashed lines), level number of samples M_ℓ (dotted lines): run 1 (multiple value curve) vs. run 2 (single value straight line).

Compared to the corresponding computations of the first moment depicted in figure 3, the MLMC-MC speedup factor increased from 7.1 to 10.8.

9. Summary and Conclusions

Monte Carlo (MC) can be interpreted as a special case of multilevel Monte Carlo (MLMC) with only one level and one discretization. MLMC, however, involves a hierarchy of discretizations that are pairwise combined to levels. For MLMC to be successful, computations on coarse discretizations need to be computationally cheap. Moreover, coarse-scale features of the physical process to be simulated need to be captured on the coarse discretizations. Unlike MC, MLMC samples on all discretizations but mostly on the coarse ones where computations are cheap. On the finest and computationally most expensive discretization where MC operates, MLMC computes only few samples.

In this work, MLMC was applied to quantify uncertainty of oil and water transport in random heterogeneous porous media. MLMC was compared to conventional MC for a two dimensional oil reservoir subject to water injection. The reservoir's logarithmic permeability y was modeled as a Gaussian random field with variances $\sigma_y = 1, 2$ and a space-stationary exponential covariance function with correlation lengths $\eta_y = 0.2, 0.4$. Estimates of the first two statistical moments of the water saturation at a specific instant in time were calculated by MLMC and MC. Comparisons between the corresponding computing times show speedups of MLMC with respect to MC that range from 5 up to 19 at equivalent accuracy. With unchanged discretizations but different σ_y and η_y, it is observed that the MLMC performance relative to MC suffers from a decrease

in logarithmic permeability correlation length and benefits from an increase in logarithmic permeability variance.

For transport, a two phase streamline solver was applied and the effect of fixing the streamline pattern during the simulation time was inspected. The fixed streamline assumption greatly reduces computational costs. For highly heterogeneous reservoirs with logarithmic permeability variance $\sigma_y^2 = 4$, the fixed streamline assumption leads to acceptable results, if compared to simulations where the streamline pattern is updated over time. For $\sigma_y^2 = 1$, however, deviations become significant.

In conclusion, applying MLMC for uncertainty quantification of two phase transport in random heterogeneous porous media can be highly profitable. For the investigated test cases, MLMC produces results of equal quality as MC at considerably lower computational costs. Apart from that, with the fixed streamline assumption, the computational cost can be substantially reduced, when dealing with highly heterogeneous porous media.

10. Acknowledgment

This work was performed as part of the ETH interdisciplinary research grant CH1-03 10-1. Florian Müller wishes to thank Siddhartha Mishra and Christoph Schwab for their advice. He is also thankful to Stefan Pauli, Jonas Sukys and Svetlana Tokareva for helpful discussions. Moreover, helpful discussions with Hamdi Tchelepi, Marco Thiele and Darryl Fenwick on streamline-based transport simulations are acknowledged.

AppendixA. Analytic Buckley-Leverett Solver

In the following, an analytical solution of the one dimensional Buckley-Leverett problem along a streamline is derived in terms of characteristics. Since f_w is a function of S_w solely, equation (11) can be rewritten as

$$\frac{\partial S_w}{\partial Q} + \frac{df_w}{dS_w}\frac{\partial S_w}{\partial V} = 0,$$

or by introducing the advection speed $a(S_w) = \frac{df_w}{dS_w}$,

$$\frac{\partial S_w}{\partial Q} + a(S_w)\frac{\partial S_w}{\partial V} = 0. \tag{A.1}$$

In order to describe characteristics $V = V(Q)$, the total derivative of $S_w = S_w(Q, V(Q))$ with respect to Q is set to zero,

$$\frac{dS_w}{dQ} = \frac{\partial S_w}{\partial Q} + \frac{\partial S_w}{\partial V}\frac{dV}{dQ} = 0.$$

By comparison with equation (A.1), the following relation is found,

$$\frac{dV}{dQ} = a(S_w).$$

Using the fact that on a characteristic curve $\frac{dS_w}{dQ} = 0$, integration yields

$$V(Q) = a(S_w)Q \quad \text{or} \quad \frac{V}{Q} = a(S_w). \tag{A.2}$$

After determining a shock between saturation S_w^* and 0 by the Rankine-Hugoniot jump condition,

$$\frac{f_w(S_w^*) - f_w(0)}{S_w^* - 0} = a(S_w^*),$$

the inversion of equation (A.2) above becomes unique,

$$S_w = a^{-1}(V/Q). \tag{A.3}$$

This yields the desired assignment of characteristic variable $\xi = V/Q$ to water saturation S_w along a streamline.

For a quadratic relative permeability $f_w(S_w)$, the inverse function in equation (A.3) is not available in closed form but can be provided numerically as a look-up table. This table describes the relation between the characteristic variable $\xi = V/Q$ and the water saturation S_w up to the shock location. In front of the shock, the table contains N_ξ points. For ξ after the shock location, $S_w = 0$. In analogy to all numerical discretization parameters in MLMC, the number of look-up table entries N_ξ is reduced for coarser grid discretizations.

AppendixB. Spectral Generator

In the following, the spectral generator to compute Gaussian random field realizations based on [19, 20, 21] is described. The generator relies on the discrete Fourier transform and its FFT implementation. To simplify matters, explanations are provided only for a one dimensional Gaussian random field with zero mean.

A vector $\boldsymbol{y}$ of N Gaussian random variables $y(n)$, $n = 0, \ldots, N-1$, with even N is assigned to a regular one dimensional grid. We assume that the correlation among different $y(n)$ can be represented by a real, symmetric, stationary and periodic covariance matrix. Such a covariance matrix does not contain more information then the kernel $\boldsymbol{C}$, $C(n) = \mathbb{E}[y(0)y(n)]$. $\boldsymbol{C}$ is a real vector with symmetry $C(n) = C(N-n)$ and unique $C(0)$ and $C(N/2)$.

The kernel $\boldsymbol{C}$ can be written as a convolution of a vector $\boldsymbol{R}$ with itself,

$$\boldsymbol{C} = \boldsymbol{R} * \boldsymbol{R} \text{ or } C(n) = \sum_{m=0}^{N-1} R(m)R(m-n), \tag{B.1}$$

using the convolution operator symbol $*$. In our case, $\boldsymbol{R}$ has the same symmetry as $\boldsymbol{C}$ and is real as well. An appropriately correlated random vector $\boldsymbol{y}$ can then be computed via

$$\boldsymbol{y} = \boldsymbol{R} * \boldsymbol{z}, \tag{B.2}$$

where $\boldsymbol{z}$ is a random vector of independent, standard normally distributed random variables (see for example [21], page 704).

Computing $\boldsymbol{y}$ is facilitated thanks to the convolution theorem for the discrete Fourier transform. Let tilde denote the respective one dimensional discrete Fourier transform, i.e. $\tilde{\boldsymbol{X}}$ is the Fourier transform of vector $\boldsymbol{X}$. Due to the convolution theorem, the Fourier transformed equation (B.1) reads

$$\tilde{\boldsymbol{C}} = \tilde{\boldsymbol{R}} \cdot \tilde{\boldsymbol{R}},$$

where $\cdot$ denotes element–wise multiplication. $\tilde{\boldsymbol{C}}$ can be computed from $\boldsymbol{C}$ with FFT and $\tilde{\boldsymbol{R}}$ from taking the element–wise square root of $\tilde{\boldsymbol{C}}$. The square root needs to be computed with care: since $\boldsymbol{R}$ is real, $\tilde{\boldsymbol{R}}$ posses Hermitian symmetry, i.e. $\tilde{R}(n) = \overline{\tilde{R}}(N-n)$, real $\tilde{R}(0)$ and real $\tilde{R}(N/2)$, where an overbar denotes complex conjugate. Equation (B.2) is also Fourier transformed,

$$\tilde{\boldsymbol{y}} = \tilde{\boldsymbol{R}} \cdot \tilde{\boldsymbol{z}}.$$

Here, $\tilde{\boldsymbol{R}}$ is known and $\tilde{\boldsymbol{z}}$ results from applying FFT to $\boldsymbol{z}$. After an inverse FFT of $\tilde{\boldsymbol{y}}$, the appropriately correlated $\boldsymbol{y}$ is found.

In general, the kernel $\boldsymbol{C}$ does not have the desired symmetry because the covariance matrix is not periodic. To overcome this problem, only the random variables $y(n)$ with $n = 0, \ldots, N/2-1$ are assumed to correspond to physical grid cells while $y(n)$ with $n = N/2, \ldots, N-1$ are dummy variables. The correlation among physical random variables, i.e. $C(n)$ with $n = 0, \ldots, N/2-1$, are defined by the physical Gaussian process under consideration. The correlations involving dummy variables, i.e. $C(n)$ with $n = N/2+1, \ldots, N-1$, establish the required symmetry in $\boldsymbol{C}$. Finally, $C(N/2)$ is used to ensure real $\tilde{R}(0)$ and $\tilde{R}(N/2)$. Assuming no negative physical correlations in $\boldsymbol{C}$, this can be achieved by computing $C(N/2)$ such that $\tilde{C}(N/2) = 0$.

AppendixC. Covariance Matrix

As described in Section 5.5, logarithmic permeability field realizations y_ℓ^i on level $\ell+1$ are calculated by cell averaging $y_{\ell+1}^i$ as indicated in figure 2. To calculate y_ℓ^i in coarse grid cell 1, i.e. $y_{\ell,1}^i$, the four values $y_{\ell+1}^i$ of the finer discretization included in coarse cell 1 are averaged, i.e.

$$y_{\ell,1}^i = \frac{y_{\ell+1,1}^i + y_{\ell+1,2}^i + y_{\ell+1,3}^i + y_{\ell+1,4}^i}{4}. \tag{C.1}$$

The statistics of averaged realizations y_ℓ^i on level $\ell+1$ must agree with realizations y_ℓ^i directly generated on level ℓ. In order to directly generate such realizations, the covariance matrix C_{y_ℓ} of process y_ℓ needs to be computed for all $\ell = 1, \ldots, L-1$. Based on the definition of the covariance

$$C_{y_\ell}(m,n) = \mathbb{E}[y_{\ell,m} y_{\ell,n}], \tag{C.2}$$

of grid cells m and n on discretization ℓ, the C_{y_L} on the finest discretization given by a geostatistical model, and the averaging expression (C.1), it is straight forward to determine C_{y_ℓ} for coarser discretizations. For example for the case illustrated in figure 2, the covariance between cells 1 and 2 on discretization ℓ results from the corresponding covariances among the cells 1 to 8 on the finer discretization $\ell + 1$,

$$C_{y_\ell}(1,2) = 1/16 \quad \Big(C_{y_{\ell+1}}(1,5) + \cdots + C_{y_{\ell+1}}(1,8) + \\ \cdots \\ C_{y_{\ell+1}}(4,5) + \cdots + C_{y_{\ell+1}}(4,8) \Big) \quad .$$

The covariance matrix on a certain discretization is therefore calculable based on the matrix on the next finer discretization. In view of the spectral random field generator described in AppendixB, it is important to note that coarse covariance matrices inherit the stationarity of the finer ones.

[1] A. G. Journel, C. Huijbregts, Mining geostatistics, Academic Press, London a.o., 1978.

[2] H. Li, D. X. Zhang, Probabilistic collocation method for flow in porous media: Comparisons with other stochastic methods, Water Resources Research 43 (2007) W09409.

[3] G. Lin, A. M. Tartakovsky, An efficient, high-order probabilistic collocation method on sparse grids for three-dimensional flow and solute transport in randomly heterogeneous porous media, Advances in Water Resources 32 (2009) 712–722.

[4] F. Müller, P. Jenny, D. Meyer, Probabilistic Collocation and Lagrangian Sampling for Advective Tracer Transport in Randomly Heterogeneous Porous Media, Advances in Water Resources 34 (2011) 1527–1538.

[5] D. X. Zhang, H. A. Tchelepi, Stochastic analysis of immiscible two-phase flow in heterogeneous media, Spe Journal 4 (1999) 380–388.

[6] D. X. Zhang, L. Y. Li, H. A. Tchelepi, Stochastic formulation for uncertainty analysis of two-phase flow in heterogeneous reservoirs, Spe Journal 5 (2000) 60–70.

[7] S. Heinrich, Multilevel Monte Carlo methods, Large-scale scientific computing, Third international conference LSSC 2001, Sozopol, Bulgaria, 2001, Lecture Notes in Computer Science 2170 (2001) 58–67.

[8] M. B. Giles, Multilevel Monte Carlo Path Simulation, Operations Research 56 (2008) 607–617.

[9] K. Cliffe, M. Giles, R. Scheichl, A. Teckentrup, Multilevel Monte Carlo methods and applications to elliptic PDEs with random coefficients, Computing and Visualization in Science 14 (2011) 3–15.

[10] A. Barth, C. Schwab, N. Zollinger, Multi-level Monte Carlo Finite Element method for elliptic PDEs with stochastic coefficients, Numerische Mathematik 119 (2011) 123–161.

[11] S. Mishra, C. Schwab, Sparse tensor multi-level Monte Carlo finite volume methods for hyperbolic conservation laws with random initial data, Math. Comp. (to appear) (2012).

[12] S. Mishra, C. Schwab, J. Sukys, Multi-level Monte Carlo finite volume methods for nonlinear systems of conservation laws in multi-dimensions., J. Comput. Physics 231 (2012) 3365–3388.

[13] M. Thiele, Streamline simulation, Seventh International Forum on Reservoir Simulation, Baden-Baden, Germany, 2003 (2003).

[14] R. Batycky, A three-dimensional two-phase field scale streamline simulator, Ph.D. thesis, Stanford University, 1997.

[15] T. Hewett, T. Yamada, Theory for the semi-analytical calculation of oil recovery and effective relative permeabilities using streamtubes, Advances in Water resources 20 (1997) 279–292.

[16] D. W. Meyer, H. A. Tchelepi, Particle-based transport model with Markovian velocity processes for tracer dispersion in highly heterogeneous porous media, Water Resources Research 46 (2010) W11552.

[17] D. W. Pollock, Semianalytical Computation of Path Lines for Finite-Difference Models, Ground Water 26 (1988) 743–750.

[18] R. J. LeVeque, Finite-Volume Methods for Hyperbolic Problems, Cambridge University Press, 2002.

[19] E. Pardo-Iguzquiza, M. Chica-Olmo, The Fourier integral method: an efficient spectral method for simulation of random fields, Mathematical Geology 25 (1993) 177–217.

[20] J. Chiles, P. Delfiner, Discrete exact simulation by the Fourier method, Geostatistics Wollongong '96, Wollongong, Australia, 1996 1 (1997) 258–269.

[21] M. Ravalec, B. Noetinger, L. Hu, The FFT moving average (FFT-MA) generator: An efficient numerical method for generating and conditioning Gaussian simulations, Mathematical Geology 32 (2000) 701–723.

Research Reports

No.	Authors/Title
12-12	*F. Müller, P. Jenny and D.W. Meyer* Multilevel Monte Carlo for two phase flow and transport in random heterogeneous porous media
12-11	*V. Kazeev, O. Reichmann and Ch. Schwab* *hp*-DG-QTT solution of high-dimensional degenerate diffusion equations
12-10	N.H. Risebro and F. Weber A note on front tracking for the Keyfitz-Kranzer system
12-09	*U. Koley and N.H. Risebro* Convergence of finite difference schemes for symmetric Keyfitz-Kranzer system
12-08	*S. Mishra, Ch. Schwab and J. Šukys* Monte Carlo and multi-level Monte Carlo finite volume methods for uncertainty quantification in nonlinear systems of balance laws
12-07	*A. Hiltebrand and S. Mishra* Entropy stable shock capturing space-time discontinuous Galerkin schemes for systems of conservation laws
12-06	*R. Hiptmair, A. Moiola and I. Perugia* Trefftz discontinuous Galerkin methods for acoustic scattering on locally refined meshes
12-05	*C. Winteler, R. Käppeli, A. Perego, A. Arcones, N. Vasset, N. Nishimura, M. Liebendörfer and F.-K. Thielemann* Magneto-rotationally driven Supernovae as the origin of early galaxy r-process elements?
12-04	*P. Grohs* Intrinsic localization of anisotropic frames
12-03	*P. Grohs* Geometric multiscale decompositions of dynamic low-rank matrices
12-02	*D. Kressner and C. Tobler* htucker - A Matlab toolbox for tensors in hierarchical Tucker format
12-01	*F.Y. Kuo, Ch. Schwab and I.H. Sloan* Quasi-Monte Carlo methods for high dimensional integration - the standard (weighted Hilbert space) setting and beyond
11-72	*P. Arbenz, A. Hiltebrand and D. Obrist* A parallel space-time finite difference solver for periodic solutions of the shallow-water equation